AUTHOR(S): IYI, D., HASAN, R. and PENLINGTON, R.

TITLE: Effect of emissivity on the heat and mass transfer of humid air in a cavity filled with solid obstacles.

YEAR: 2015

Publisher citation: IYI, D., HASAN, R. and PENLINGTON, R. 2015. Effect of emissivity on the heat and mass transfer of humid air in a cavity filled with solid obstacles. Numerical heat transfer, part A: applications [online], 67(5), pages 531-546. Available from: https://doi.org/10.1080/10407782.2014.937261

OpenAIR citation: IYI, D., HASAN, R. and PENLINGTON, R. 2015. Effect of emissivity on the heat and mass transfer of humid air in a cavity filled with solid obstacles. Numerical heat transfer, part A: applications [online], 67(5), pages 531-546. Available from: https://doi.org/10.1080/10407782.2014.937261

Numerical Heat Transfer, Part A, 67: 1–16, 2015

ISSN: 1040-7782 print/1521-0634 online
DOI: 10.1080/10407782.2014.937261

Taylor & Francis
Taylor & Francis Group

EFFECT OF EMISSIVITY ON THE HEAT AND MASS TRANSFER OF HUMID AIR IN A CAVITY FILLED WITH SOLID OBSTACLES

Draco Iyi, Reaz Hasan, and Roger Penlington
Faculty of Engineering and Environment, Department of Mechanical and Construction Engineering, Northumbria University, Newcastle Upon Tyne, UK

The work reported here is a 2D numerical study on the buoyancy-driven low-speed turbulent flow of humid air inside a rectangular cavity partially filled with solid cylindrical objects for a Rayleigh number of 1.45×10^9. Variations of Nusselt number, buoyancy flux, vapor mass fraction, and turbulence viscosity ratio are presented for various emissivity values of wall surfaces. It was observed that during the natural convection process, radiation effects are very significant and the air/water vapor combination results in a small increase in heat transfer as compared with the pure natural convection of dry air.

1. INTRODUCTION

Buoyancy-driven flow inside cavities has been the subject of extensive research for the last two decades due to the growing demand for detailed quantitative knowledge of the transfer processes and also due to its relevance in many practical applications [1, 2]. The basic setup for such flows, which has also attracted most attention from researchers, is a rectangular cavity filled with dry air whose opposing vertical walls are heated differentially [3, 4]. Detailed data on flow, turbulence, and heat transfer have been collected through various experiments [5–7]. Following this, numerical researchers have also been quick to respond to the experimental literature by conducting validation and exploratory studies on this very topic [8]. The interest seems to be ongoing because more challenging situations are emerging with time [7, 9].

In the case of a rectangular cavity of height H, the natural convection heat transfer from hot to cold walls is characterized by the formation of a slowly moving vortex. This vortical motion is often interpreted as an "engine" which transfers heat from the heated surface (source) to the cold surface (sink). The intensity of the flow is conveniently expressed by the Rayleigh number, $Ra = g\beta\Delta T H^3/(\alpha v)$, where β is the coefficient of thermal expansion and ΔT is the temperature difference between the vertical walls. Depending on the Rayleigh number, the flow can be treated as

Received 12 September 2013; accepted 18 June 2014.
Address correspondence to Reaz Hasan, Faculty of Engineering and Environment, Department of Mechanical and Construction Engineering, Northumbria University, Newcastle Upon Tyne NE1 8ST, UK. E-mail: reaz.hasan@northumbria.ac.uk

NOMENCLATURE

A	heat transfer area (m^2)	$\vec{v}$	velocity vector (m/s)
B	buoyancy flux (m^2/s^3)	V_y	vertical velocity component (m/s)
D_{eff}	effective diffusion coefficient (m^2/s)	x	species concentration
g	gravitational acceleration (m/s^2)	x, y	coordinates in x- and y-directions
Gr	Grashof number, ($=g\beta\Delta TL^3/\nu^2$)	y^+	nondimensional wall distance
H	height of the cavity (m)	α	absorption coefficient ($=k/\rho c_p$)
k	thermal conductivity (W/m K)	β	thermal expansion coefficient (1/K)
L	width of the cavity (m)	δ	wall proximity (m)
m	mass fraction of vapor to dry air	ΔT	temperature difference
M	molecular weight of vapor	σ	Stefan–Boltzmann constant ($5.672 \times 10^{-8}\,W/m^2\,K^4$)
N	buoyancy number		
Nu	local Nusselt number	ρ	density (kg/m^3)
P	pressure (Pa)	μ	dynamic viscosity (kg/ms)
Pr	Prandtl number	ε	turbulent dissipation rate (m^2/s^3)
Ra	Rayleigh number ($=g\beta\Delta TH^3/\mu\alpha$)	ε	emissivity
T	temperature (K, °C)	Ψ	stream function (kg/s)

turbulent or laminar. Rayleigh numbers lower than 10^8 indicate a buoyancy-induced laminar flow, with transition to turbulence occurring over the range of $10^8 < Ra < 10^{10}$ [10, 11].

In the last decade or so, the trend in buoyancy-driven flow research has shifted to the examination of cavity flow coupled with heat and mass transfer [2, 12]. The majority of studies in this category are concentrated on steady-state laminar flow of Rayleigh numbers over the range 10^4–10^6 [13] investigating the flow induced by temperature and mass concentration gradient. A single-phase modeling approach for the transport of fluid mixture for laminar flows was used. On the other hand, numerical works carried out by Teodosiu et al. [14] and Close and Sheridan [15] assumed a two-phase laminar flow for the transport of fluid mixture, which highlights the influence of concentration gradient upon the development of the flow.

A more recent shift in the study of buoyancy-driven cavity flow is to examine the simultaneous heat and mass transfer in enclosures containing solid obstacles. This interest has grown due to its relevance to practical flows such as comfort in indoor environments [8], design of double skin facades [16], the drying/cooling of agricultural products [1], cold storage, and other engineering applications [17]. Unlike porous media, these obstacles are not in contact with each other but are close enough to influence the transfer processes significantly. Typical examples of studies in this category are the works by Das and Reddy [18], Desrayaud and Lauriat [13], and Yoon et al. [19], all of which are limited to steady-state two-dimensional laminar natural convection flow of Rayleigh number ranging from 10^5 to 10^8. Das and Reddy [18] and Yoon et al. [19] have reported on fluid flow and heat transfer in a differentially heated rectangular cavity containing just one disconnected solid product, and Bragas and de Lemos [20, 21] and Hooman and Merrikh [22] investigated cavities filled with several obstacles. Findings from these research works show that when a limited number of solid products are involved, fluid flow is predominantly confined between the vertical walls and the first column of the objects. Further, an

increase in the number of solid products results in greater fluid flow in some areas, especially close to the product surfaces.

Another important characteristic of this kind of flow is the importance of radiation between surfaces. It is known [23] that the effect of radiation is fairly significant and comparable to convective heat transfer even for moderately low temperature differences in naturally ventilated spaces. In this context, surface emissivity plays a very important role in establishing total heat transfer. Laguerre et al. [17] reported on a study for a Rayleigh number of 1.45×10^9. The numerical calculations were based on the assumption that the flow is laminar, but in reality this *Ra* may be considered to be in transition to the turbulent regime. The effect of radiation between the walls and the solid objects has been given special attention and the findings highlight this contribution. However, the study considered only one value of emissivity for the prediction of the experimental data.

The aims of the present numerical study are to explore the detailed flow field for humid air in a rectangular cavity with solid obstacles, which was also the test case for Laguerre et al. [17]. Of particular interest in our study is analysis of the influence of the surface emissivity of the cavity walls and of the solid obstacles in an effort to quantify radiation influences. Also, we have scrutinized the flow by considering it to be turbulent. Finally, the effect of humidity was also studied in detail with a view to quantifying the exact contributions due to concentration gradient.

2. FLOW PROBLEM

The geometrical configuration used in this investigation is similar to the cavity used in the experimental study conducted by Laguerre et al. [17]. As shown in Figure 1, this is a two-dimensional rectangular cavity with an aspect ratio of 2:1 (H/L) and contains obstacles which occupy about 15% of the total cavity volume.

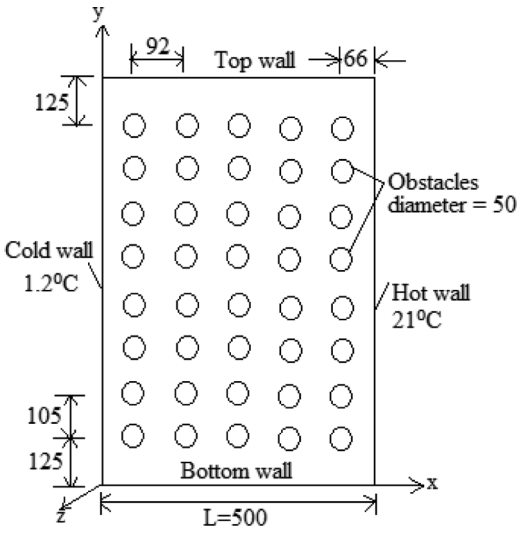

Figure 1. Geometry and the coordinates (dimensions are in mm).

The temperatures of the vertical walls were maintained at 1.2°C and 21°C (i.e., $\Delta T = 19.8$°C). The authors have provided data for temperature profiles along the mid-height ($y/H = 0.5$) and at $x = 66$ mm near the cold wall of the cavity. Vertical velocity (V_y) and relative humidity profiles measured at the mid-height and mid-width ($x/L = 0.5$) of the cavity were also reported. In the experimental setup, humidity was maintained by placing a shallow pan of water (13.7°C) at the bottom surface which was heated electrically. The temperatures of all the walls along with other relevant properties were all available in the article.

3. NUMERICAL METHOD

Calculations were carried out using the commercial Computational Fluid Dynamics software FLUENT: *ANSYS® Academic Research, Release 13.0*. The methodology involves the iterative solution of the Navier–Stokes equations along with continuity and energy equations using the SIMPLE algorithm on collocated variables. Humidity was considered as a separate phase and hence another scalar transport equation for species transport was incorporated. We assumed the flow to be turbulent and hence suitable two-equation eddy-viscosity turbulence models were also chosen. More details on turbulence models will be given in the next section. Without going into detailed description of the governing differential equations which may be found in several text books such as Versteeg and Malalasekera [24], we concentrate on the numerical strategies and accuracy aspects of the predictions. However, for the sake of completeness the governing equations for mass, momentum, energy, and species concentration are given as follows.

$$\vec{\nabla} \cdot (\rho \vec{v}) = 0 \tag{1}$$

$$\vec{\nabla} \cdot (\rho \vec{v} \otimes \vec{v}) = - \vec{\nabla} p + \mu \vec{\nabla} \cdot \left[\vec{\nabla} \cdot \vec{v} + \left(\vec{\nabla} \cdot \vec{v} \right)^T - \frac{2}{3} \left(\vec{\nabla} \cdot \vec{v} \right) I \right] + (\rho - \rho_0) \vec{g} \tag{2}$$

$$C_p \vec{\nabla} \cdot (\rho T \vec{v}) = \lambda \vec{\nabla}^2 T \tag{3}$$

$$\vec{\nabla} \cdot (\rho x \vec{v}) = D \vec{\nabla} \cdot \left(\rho \vec{\nabla} x \right) \tag{4}$$

From a numerical analysis point of view, the accuracy of computations is affected by the choice of grids, the viscous models, discretization schemes, and the convergence criteria and remains a major concern for numerical scientists [8, 25]. These uncertainties that may influence the flow physics were carefully taken into account in the numerical modeling for greater accuracy. For discretization of the convection terms, second-order convection schemes were considered. Utmost care was taken to address the issues of grid density and grid quality. The mesh was made up of structured quad mesh near the walls and unstructured near the core region, where the flow velocity is very low.

In order to capture the sharp gradients, the mesh was clustered near the walls, where minimum mesh orthogonal quality was about 1. (A value close to zero indicates low-quality mesh and a value close to one indicates high-quality mesh.)

Particular attention was given to resolve the boundary layer very close to the walls because of the low-*Re* turbulence models that were used for the simulations. The number of cells in the first layer of each cylindrical obstacle in the circumferential direction was initially 40, which was then raised to 68 corresponding to an overall mesh density of 90,500. The results were generally insensitive to the changes of grid density around obstacles; hence all the calculations reported in this article were obtained with this mesh. The value of the nondimensional distance, y^+ for the final mesh, was found to be just below 1 for all surfaces (cavity and solid obstacles), justifying our use of the low-*Re* model.

It is worthwhile to note that the process of computing a steady-state solution using very fine mesh had been quite challenging because of oscillations associated with higher-order discretization schemes. As a result, a number of steps were taken to achieve a steady-state solution. Initially, a natural convection flow field was established with a lower value of Rayleigh number (10^6) with a first-order convection scheme using an incompressible unsteady solver for a time step of 0.002 s. This flow field was later used as an initial condition for the higher Rayleigh number of 1.45×10^9 with the second-order discretization schemes for all equations. Calculations were performed using a single Intel core 2Duo E6600 2.4 GHz processor and a typical run took about 8 h of computing time.

The boundary conditions considered for the simulations are similar to those given in the experimental paper of Laguerre et al. [17] and are summarized in Table 1. The constant vapor mass fraction is maintained at the bottom horizontal wall and impermeable conditions assumed for the top and hot vertical walls and for the surfaces of cylindrical obstacles. To conserve the species transport equation, a constant mass fraction equal to the saturation value at the cold wall was specified. The condition of constant mass fraction at the cold wall is justified because the temperature is constant on that surface. No slip boundary conditions were imposed for any solid surfaces.

Finally, to simulate the heat transfer due to radiation, the discrete ordinate method [26] was chosen due to its proven superiority in predicting radiative heat transfer involving a participating medium. In this study, the humid air is treated as an absorbing–emitting and nonscattering gray medium. The general equation of heat transfer by radiation (in a given $\vec{s}$ direction) for both unhumidified and humidified cavities is

$$\vec{\nabla} \cdot (I(\vec{r}, \vec{s})\vec{s}) = 0 \tag{5}$$

Table 1. Boundary conditions used in the simulations

Wall	Thermal conditions (°C)	Mass fraction (kg water/kg air)	Material, thermal conductivity (W/m K)
Top	14.4	Zero diffusive flux	Plaster, 0.35
Bottom	13.7	0.00968	Plaster, 0.35
Cold	1.2	0.00407	Aluminum, 202.4
Hot	21	Zero diffusive flux	Glass, 0.75
Obstacles	Zero heat flux	Zero diffusive flux	Plaster, 0.35

where $I(\vec{r},\vec{s})$ is the radiative intensity in the $\vec{s}$ direction and $\vec{r}$ is the position vector. At the surface of the solid obstacles, the thermal boundary condition is

$$-\lambda\ \vec{\nabla}T\cdot\vec{n}+\text{Ø}_{\text{net.rad}}=-\lambda\ \vec{\nabla}T_p\cdot\vec{n} \tag{6}$$

where $\text{Ø}_{\text{net.rad}}=\text{Ø}_{\text{in}}-\text{Ø}_{\text{out}},\text{Ø}_{\text{in}}=\int_{\vec{s}\cdot\vec{n}>0}I_{\text{in}}\cdot\vec{s}\cdot\vec{n}\cdot\mathrm{d}\Omega,\text{Ø}_{\text{out}}=(1-\varepsilon_r)\cdot\text{Ø}_{\text{in}}+\varepsilon_r\sigma T_p^4$.

The walls are all assumed as gray diffuse and four angles of discretization (2, 4, 16, and 24) were used.

4. RESULTS AND DISCUSSION

4.1. Choice of Viscous Model

At the very outset of this investigation, we decided to evaluate whether the flow should be considered laminar or turbulent and at the same time to scrutinize the sensitivity of common viscous models. This was felt necessary due to the fact that the Rayleigh number is 1.45×10^9, which is clearly within the transition zone [27]. For practical reasons, we restricted ourselves to six popular eddy viscosity models available within the FLUENT package. These are abbreviated as AKN (Abe et al. [28]) AB (Abid [29]), CHC (Chang et al. [30]), LM (Lam and Bremhost [31]), LS (Launder and Sharma [32]), and YS (Yang and Shih [33]). Figures 2*a, b* show the velocity profiles predicted by various models along the mid-height of the cavity.

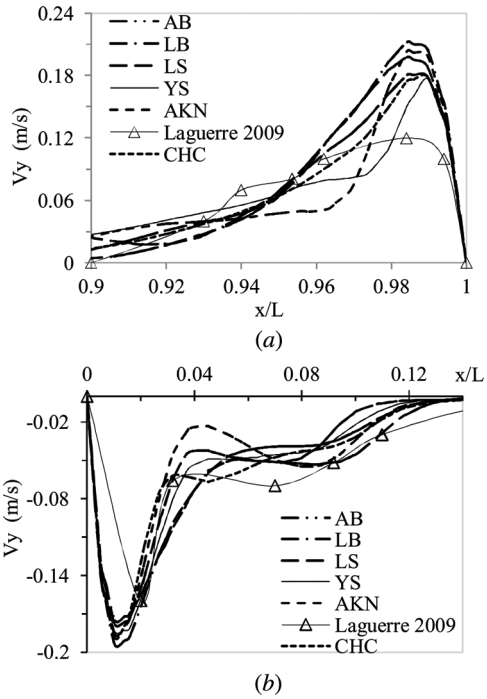

Figure 2. Profiles at mid-height (*a*) vertical velocity near the hot wall; (*b*) vertical velocity near the cold wall.

A careful examination at the velocity profiles reveals that while the core region outside the boundary layers is fairly stagnant and hence insensitive to the turbulence models, the situation is very different near the vertical walls. The Launder–Sharma model returned the best overall results and hence this has been used for all the calculations reported in this work. Figures 3*a, b* compare the temperature profile near the cold wall ($x = 66$ mm) and the relative humidity distribution along the mid-width ($x = 0.5\ L$). Results obtained with the laminar assumption were plotted and both figures justify our approach to incorporate a turbulence model.

4.2. 2D Simplification of 3D Radiation

The choice of emissivity is critical when modeling radiation heat transfer and, even for this type of moderate temperature difference, the effect of radiation has been found to be fairly significant. The 2D simplification of an inherently 3D radiation heat transfer also raises issues about the accuracy of the data produced by 2D simplification of the domain. According to Laguerre et al. [17], the presence of the side wall in the experimental setup was "unavoidable", the net effect of which was, to some extent, equivalent to "shielding" of radiation which the 2D geometries cannot replicate. They further argued that for a 2D calculation with all surfaces having the same emissivity, the emissivity ε_{2D} can be equated to ε_{3D} by the following relation:

$$\varepsilon_{2D} = \frac{2\varepsilon_{3D}}{(4 - \varepsilon_{3D})} \tag{7}$$

Laguerre [17] predictions with equivalent ε_{2D} values instead of ε_{3D} are far better than those with actual surface emissivity. With this simplified relation, the emissivity of $\varepsilon_{3D} = 0.9$ for all surfaces gives an equivalent emissivity of $\varepsilon_{2D} = 0.58$. We scrutinized this simplification further and a comparison of temperature for 2D vs. 3D domains is presented in Figure 4. It will be seen that the predicted temperatures at $x/L = 0.5$ for $\varepsilon = 0.9$ (3D) and $\varepsilon = 0.58$ (2D) are in close agreement, justifying the need for a smaller emissivity value for 2D calculation. The value $\varepsilon = 0.9$ (2D) is shown for comparison, which also highlights the significant influence of radiation for this flow.

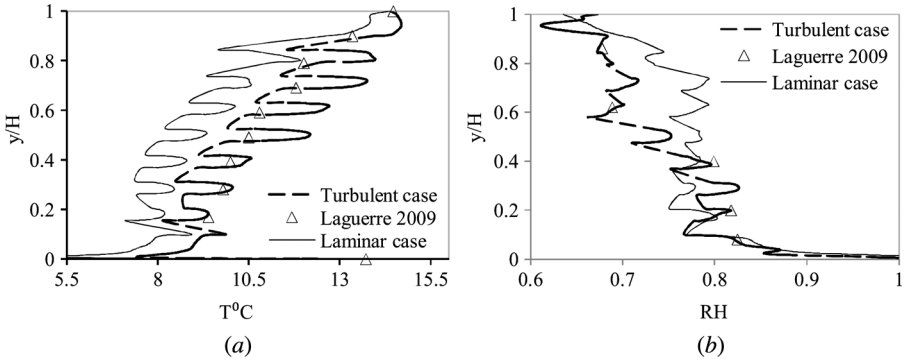

Figure 3. (*a*) Profiles of temperature at 66 mm from the cold wall; (*b*) profile of relative humidity at mid-width.

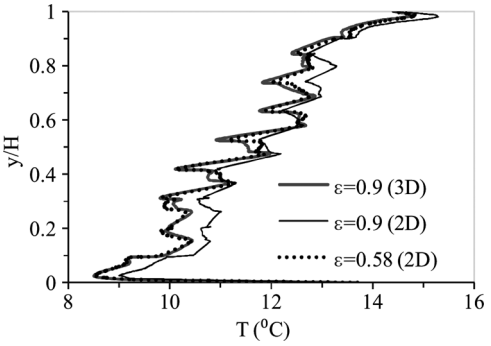

Figure 4. Emissivity sensitivity for temperature prediction.

As mentioned in the "Introduction" section, one of the aims of this article is to study the effect of surface emissivity on various flow features. In light of the above discussion, we decided to present the results for four emissivity values of $\varepsilon = 0$, 0.22, 0.58, and 0.67 for our 2D model, which correspond to $\varepsilon = 0$, 0.4, 0.9, and 1.0, respectively, for the 3D model. It is fully recognized that this simplification needs further analysis but the results presented later will not be affected because we are interested in the trends. Although we did perform calculations with higher values of ε for the 2D domain, they have not been included for reasons of clarity.

4.3. Temperature Fields

Temperature distribution is one of the most critical mean quantities, because the flow develops as a result of buoyancy which is directly dependent upon the temperature gradient. Concentration gradient also plays a part but as will be shown later that it is much less dominant. Figures 5*a, b* show the temperature plots along the mid-width ($x = 0.5\ L$) and near the cold wall ($x = 66$ mm), respectively. It will be seen that temperature stratification is lower at the bottom wall and higher at the top wall for all values of emissivity. Since radiation between all surfaces is considered, oscillations of the temperature profiles can be very clearly seen in these plots. This

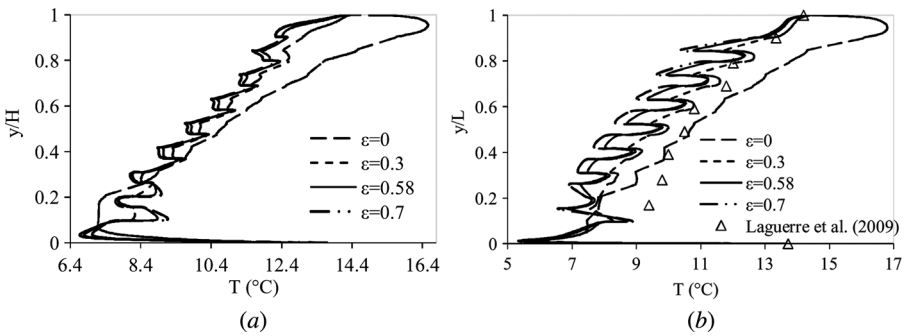

Figure 5. Temperature profile at (*a*) mid-width; (*b*) near cold wall ($x = 66$ mm).

is because the fluid temperature further away from the cylinder surface is higher than that very close to its surface – a phenomenon highly influenced by the surface emissivity value.

The temperature profile of the flow domain shows a decrease in temperature with the increase in emissivity. In addition to the overall thermal stratification in the cavity, stratification is also observed in each gap between the obstacles. One very important point to note is the fact that the predicted temperature for $\varepsilon = 0$ (i.e., without radiation) is very inaccurate, the largest discrepancy being displayed near the top wall. This has also been numerically verified by Laguerre et al. [17]. The fact that the inclusion of radiation improves the results drastically is a further verification that radiation does play a very significant role in apparently low-temperature applications.

4.4. Wall Heat Transfer

The rate of heat transfer at each wall is determined by the arithmetic sum of convection and radiation components for both local and average values. Equation (8*a*) shows the expression for the local Nusselt number:

$$(Nu = Nu_{\text{cov}} + Nu_{\text{rad}}) \tag{8a}$$

In Eq. (8*a*), Nu represents the total local Nusselt number which is made up of $Nu_{\text{cov}} = q_{i_{\text{rad}}} L/\bar{k}\Delta T$ and $Nu_{\text{rad}} = q_{i_{\text{rad}}} L/\bar{k}\Delta T$, where q_i is the local convective heat flux and $q_{i_{\text{rad}}}$ is the radiative heat flux evaluated at each node (ith node) along a given wall.

Similarly, the average Nusselt number is given by Eq. (8*b*) below:

$$\overline{Nu} = \overline{Nu}_{\text{cov}} + \overline{Nu}_{\text{rad}} \tag{8b}$$

In Eq. (8*b*), Nu represents the average heat transfer for the wall and is made up of $\overline{Nu}_{\text{cov}} = \bar{q}_{\text{cov}} L/\bar{k}\Delta T$ and $\overline{Nu}_{\text{rad}} = \bar{q}_{\text{rad}} L/\bar{k}\Delta T$, where $\bar{q}_{\text{cov}}$ and $\bar{q}_{\text{rad}}$ are the integral average of total heat flux and radiation heat flux, respectively.

The average Nusselt numbers for the various emissivity values are shown in Table 2. It will be seen from the hot wall values that the rate of heat transfer increases with increase in emissivity. Without radiation there is a balance between the conductive and convective heat fluxes at the interfaces of the walls. Radiation causes an additional heat flux towards the interface due to incident radiation and an extra outgoing heat flux associated with emission of radiation. To ascertain the

Table 2. Average surface Nusselt number

Test	Hot	Top	Cold	Bottom
$\varepsilon = 0$	38.98	23.69	39.51	24.24
$\varepsilon = 0.22$	46.78	34.14	47.22	34.61
$\varepsilon = 0.58$	50.81	35.77	51.02	35.99
$\varepsilon = 0.7$	52.47	37.48	53.31	38.37

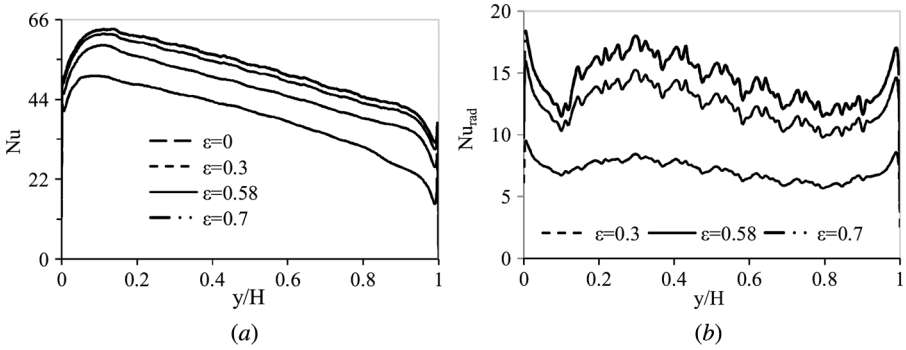

Figure 6. (*a*) Local Nusselt number along the hot wall; (*b*) local radiation Nusselt number along the hot wall.

significance of the radiation component, the local Nusselt numbers for the hot wall are plotted in Figures 6*a*, *b*. The perturbations in the radiation component are due to the proximity of the obstacles. It is also clear that the effect of emissivity is more prominent for radiation as shown in Figure 6*b*. Since the flow velocities are small (Figures 2*b*, *c*) and temperatures are low, the radiative heat fluxes are modest but comparable in size to convective heat fluxes. The local Nusselt number variation for the top wall as shown in Figure 7 indicates that heat is transferred through this wall in both directions, which is a consequence of boundary condition. The assumption of adiabatic wall which is sometimes used [5] is far from reality.

4.5. Stream Function and Turbulence

Further insight into the effect of emissivity on velocity can be obtained from the stream function plots in Figures 8*a*, *b*. As the value of emissivity is increased, there is a corresponding increment in the value of the stream function. Figure 8*a* also displays a stable (rather stagnant) zone in the core areas but shows a 45% increase in circulation rate due to emissivity increase at the midpoint measured at the

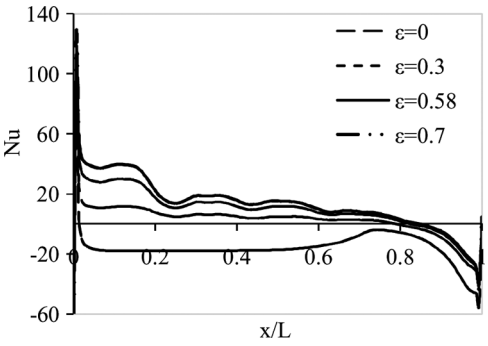

Figure 7. Local Nusselt number along the top wall.

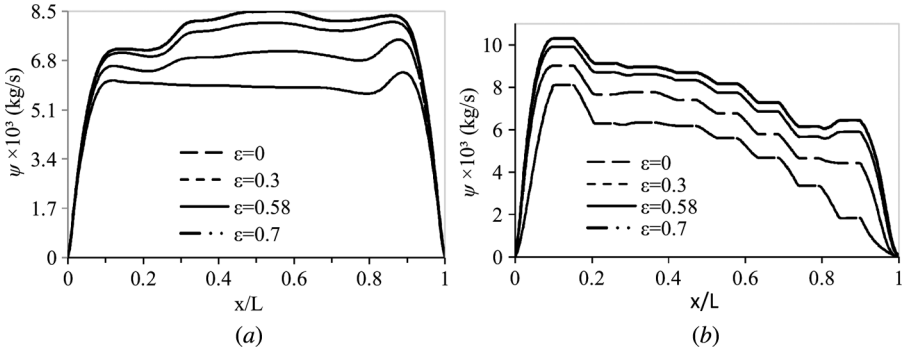

Figure 8. Stream function profile at (*a*) mid-height, (*b*) mid-width.

mid-height of the cavity. Slightly enhanced perturbations for higher ε values are the direct results of radiation. The stream function profile in Figure 8*b* shows a rather monotonically decreasing trend with peak values near the bottom wall of the cavity. The sensitivity to emissivity is fairly comparable to Figure 8*a*.

As was shown in Figures 2*b*, *c*, the flow is characterized by upward and downward boundary layer flows along the hot and cold walls, respectively, with a somewhat stagnant region in the central part. Hence the turbulent quantities are also dominant along the two walls. To analyze this effect, we plotted the turbulent viscosity ratio, $\mu^* = \mu_t/\mu$ at the mid-height of the cavity in Figure 9. As expected, the values of μ^* are only significant within the boundary layers. Interestingly, for higher ε values μ^* is found to decrease slightly. To investigate this, we plotted the components of Nusselt numbers for hot and cold walls in Figure 10 for various values of ε. It will be seen clearly that as the value of emissivity is increased, there is an adjustment between the convection and radiation components with the latter contributing to the overall increase in heat transfer. In fact, the convection component, which is affected by viscous effects, can be seen to decrease slightly (more for the cold wall) with increase in emissivity which is in line with the μ^* variation for different emissivities.

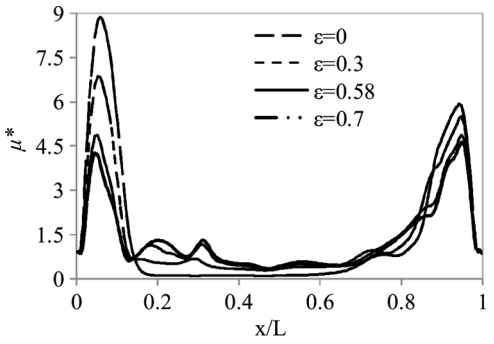

Figure 9. Turbulent viscosity ratio at mid-height.

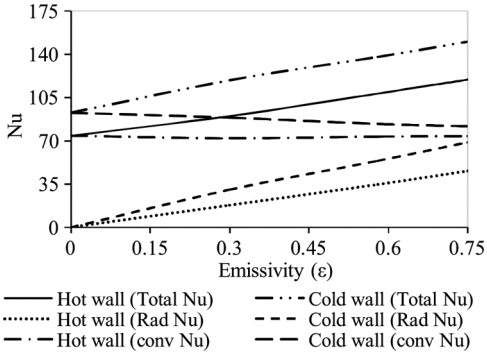

Figure 10. Total, convective, and radiative heat transfer as a function of emissivities at the hot and cold walls.

4.6. Buoyancy and Concentration Effect

Buoyancy flux B characterizes the buoyancy-driven flow and is expressed as

$$B = \frac{g\beta_{\text{mix}} q_i}{\rho c_p} \tag{9}$$

In Eq. (9), β_{mix} represents the combined volumetric expansion coefficient of the air–water vapor mixture. Figure 11 shows the buoyancy flux plot along the hot wall. As the expression for B shows, the curves follow the trend of the local Nusselt number. The buoyancy effects are the results of combined temperature and concentration gradients. The concentration gradient is due to a difference in the relative molecular mass between the dry air and water vapor. At 20°C, the relative molecular mass of dry air is 28.97 kg/kg mol, while for saturated air it is 28.71 kg/kg mol. However, water vapor is less dense and the relative molecular mass is only 18.015 kg/kg mol.

Calculations were carried out for an unhumidified cavity by considering only dry air. A comparison of the average heat transfer between the temperature-induced buoyancy (unhumidified cavity) and that due to the combined influence of mass

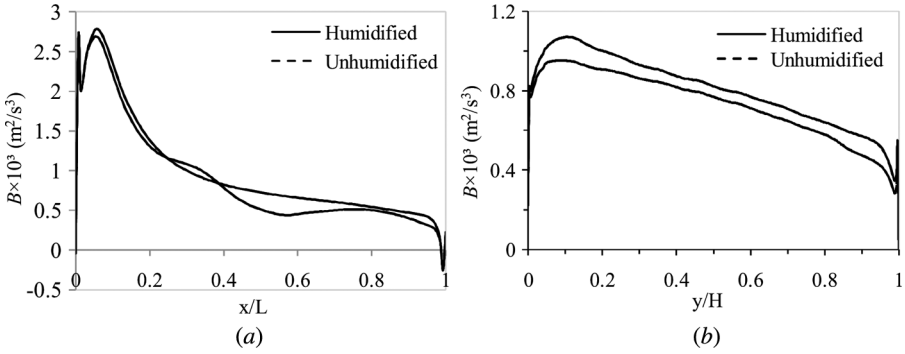

Figure 11. Buoyancy flux near (*a*) the bottom wall, (*b*) the hot wall.

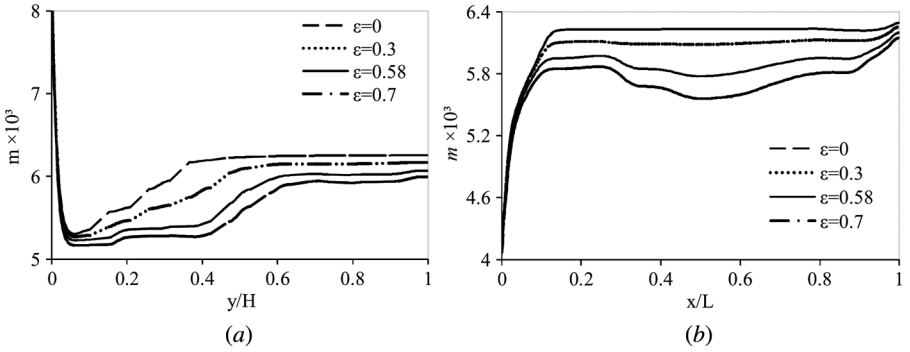

Figure 12. Mass fraction of water vapor along (*a*) mid-width, (*b*) mid-height.

and temperature (humidified cavity) was made. The difference between the two predictions was, as expected, not unduly high but not insignificant either. The data showed heat transfer enhancement of 5.4% and 5.7% for the hot and bottom walls, respectively. This observation may prove to be significant for long-exposure situations typical of human comfort studies.

Finally, we analyzed the effect of radiation on mass transfer. Figures 12*a, b* show that the mass fraction, m, defined as the ratio of mass of vapor to the total mass of mixture, decreases with increasing surface emissivity. This is due to the fact that at low emissivity value the vapor mass transfer increases, and as the emissivity value increases the fluid temperature decreases (Figures 5*a, b*).

These phenomena also account for the decrement in the profiles of the effective diffusion coefficient, D_{eff} of vapor at higher values of surface emissivity, as shown in Figure 13. Further quantitative information is provided in Figure 14, where we plotted the buoyancy number, N, which is a ratio of mass to temperature-induced buoyancy. This ratio N measures the significance of the contribution to buoyancy of the variation in vapor concentration in the cavity. The effective diffusion coefficient of vapor is also observed to be maximum close to the vertical walls and almost constant at the core of the cavity, and is comparable to the commonly used value of $\sim 3 \times 10^{-5}\,\text{m}^2/\text{s}$ [14]. As expected, the variations and nature of these curves

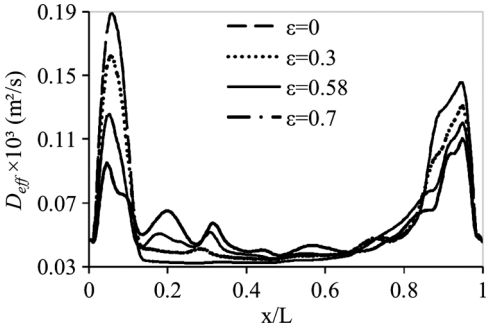

Figure 13. Effective diffusion coefficient of water vapor at mid-height.

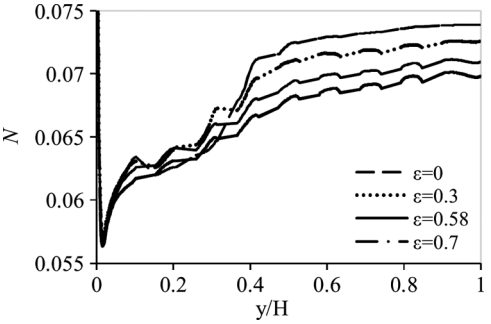

Figure 14. Ratio of mass to temperature-induced buoyancy (*a*) mid-height, (*b*) near cold wall ($x = 66$ mm).

are very similar to the viscosity ratio curves presented in Figure 9, highlighting the fundamental similarity in the diffusive transport mechanism of momentum and concentration.

5. CONCLUSIONS

The work presented in this article highlights the fact that turbulent natural convection flow is very sensitive to the appropriate choice of turbulence models. Both surface emissivity and mass concentration are found to influence heat transfer which in turn affects the fluid flow pattern inside the cavity. From our calculations, the following conclusions can be made:

- The flow field is influenced by turbulence near the walls while the core area is essentially a stagnant region. Comparison to experimental data highlights that the flow and heat transfer are better predicted with a suitable low-*Re* turbulence model. Amongst the six Eddy Viscosity Models (EVMs) employed for the predictions, the Launder–Sharma model gave the best overall result.
- Radiation was found to influence the flow, temperature, humidity, and rates of heat and mass transfer within the cavity. The implication is that by a careful selection of material, heat transfer may be passively influenced.
- Humidity affects the heat transfer rate to a limited extent, which may be relevant for long exposure in comfort designs.

REFERENCES

1. S. Kadem, A. Lachemet, R. Younsi, and D. Kocaefe, 3d-Transient Modeling of Heat and Mass Transfer During Heat Treatment of Wood, *Int. Commun. Heat Mass Transfer*, vol. 38, pp. 717–722, Jul 2011.
2. O. Laguerre, S. Ben Amara, and D. Flick, Experimental Study of Heat Transfer by Natural Convection in a Closed Cavity: Application in a Domestic Refrigerator, *J. Food Eng.* vol. 70, pp. 523–537, Oct 2005.
3. B. Calcagni, F.Marsili, and M. Paroncini, Natural Convective Heat Transfer in Square Enclosures Heated from Below, *Appl. Therm. Eng.* vol. 25, pp. 2522–2531, Nov 2005.

4. Y. S. Tian and T. G. Karayiannis, Low Turbulence Natural Convection in an Air Filled Square Cavity - Part II: The Turbulence Quantities, *Int. J. Heat Mass Transfer* vol. 43, pp. 867–884, Mar 2000.
5. F. Ampofo and T. G. Karayiannis, Experimental Benchmark Data for Turbulent Natural Convection in an Air Filled Square Cavity, *Int. J. Heat Mass Transfer* vol. 46, pp. 3551–3572, Sep 2003.
6. A. A. DafaAlla and P. L. Betts, Experimental Study of Turbulent Natural Convection in a Tall Air Cavity, *Exp. Heat Transfer* vol. 9, pp. 165–194, Apr–Jun 1996.
7. F. Penot, O. Skurtys, and D. Saury, Preliminary Experiments on the Control of Natural Convection in Differentially-Heated Cavities, *Int. J. Therm. Sci.*, vol. 49, pp. 1911–1919, 2010.
8. W. Chen and W. Liu, Numerical and Experimental Analysis of Convection Heat Transfer in Passive Solar Heating Room with Greenhouse and Heat Storage, *Sol. Energy*, vol. 76, pp. 623–633, 2004.
9. D. Saury, N. Rouger, F. Djanna, and F. Penot, Natural Convection in an Air-Filled Cavity: Experimental Results at Large Rayleigh Numbers, *Int. Commun. Heat Mass Transfer* vol. 38, pp. 679–687, Jul 2011.
10. G. Barakos, E. Mitsoulis, and D. Assimacopoulos, Natural-Convection Flow in a Square Cavity Revisited–Laminar, and Turbulent Models with Wall Functions, *Int. J. Numer. Methods Fluids*, vol. 18, pp. 695–719, Apr 15, 1994.
11. Y. Jaluria, *Natural Convection*, Pergamon Press, , Oxford, 1980.
12. G. D. McBain, Natural Convection with Unsaturated Humid Air in Vertical Cavities, *Int. J. Heat Mass Transfer* vol. 40, pp. 3005–3012, Sep 1997.
13. G. Desrayaud and G. Lauriat, Heat and Mass Transfer Analogy for Condensation of Humid Air in a Vertical Channel, *Heat Mass Transfer* vol. 37, pp. 67–76, Jan 2001.
14. C. Teodosiu, R. Hohota, G. Rusaouen, and M. Woloszyn, Numerical Prediction of Indoor Air Humidity and Its Effect on Indoor Environment, *Build. Environ.* vol. 38, pp. 655–664, May 2003.
15. D. J. Close and J. Sheridan, Natural Convection in Enclosures Filled with a Vapour and a Non-Condensing Gas, *Int. J. Heat Mass Transfer*, vol. 32, pp. 855–862, 1989.
16. F. Kuznik, T. Catalina, L. Gauzere, M. Woloszyn, and J. J. Roux, Numerical Modelling of Combined Heat Transfers in a Double Skin Facade–Full-Scale Laboratory Experiment Validation, *Appl. Therm. Eng.*, vol. 31, pp. 3043–3054, Oct 2011.
17. O. Laguerre, S.Benamara, D. Remy, and D. Flick, Experimental and Numerical Study of Heat and Moisture Transfers by Natural Convection in a Cavity Filled with Solid Obstacles, *Int. J. Heat Mass Transfer* vol. 52, pp. 5691–5700, Dec 2009.
18. M. K. Das and K. S. K. Reddy, Conjugate Natural Convection Heat Transfer in an Inclined Square Cavity Containing a Conducting Block, *Int. J. Heat Mass Transfer* vol. 49, pp. 4987–5000, Dec 2006.
19. H. S. Yoon, D. H. Yu, M. Y. Ha, and Y. G. Park, Three-Dimensional Natural Convection in an Enclosure with a Sphere at Different Vertical Locations, *Int. J. Heat Mass Transfer* vol. 53, pp. 3143–3155, Jul 2010.
20. E. J. Braga and M. J. S. de Lemos, Laminar Natural Convection in Cavities Filled with Circular and Square Rods, *Int. Commun. Heat Mass Transfer* vol. 32, pp. 1289–1297, Nov 2005.
21. E. J. Braga and M. J. S. de Lemos, Heat Transfer in Enclosures Having a Fixed Amount of Solid Material Simulated with Heterogeneous and Homogeneous Models, *Int. J. Heat Mass Transfer* vol. 48, pp. 4748–4765, Nov 2005.
22. K. Hooman and A. A. Merrikh, Theoretical Analysis of Natural Convection in an Enclosure Filled with Disconnected Conducting Square Solid Blocks, *Transp. Porous Media* vol. 85, pp. 641–651, Nov 2010.

23. M. Behnia, J. A. Reizes, and G. D. Davis, Combined Radiation and Natural-Convection in a Rectangular Cavity with a Transparent Wall and Containing a Non-Participating Fluid, *Int. J. Numer. Methods Fluids* vol. 10, pp. 305–325, Feb 1990.
24. H. K. Versteeg and W. Malalasekera, *An Introduction to Computational Fluid Dynamics: The Finite Volume Method,* 2nd ed., Pearson Education Ltd., Harlow, 2007.
25. D. A. Iyi, R. Hasan, and R. Penlington, Interaction Effects Between Surface Radiation and Double-Diffusive Turbulent Natural Convection in an Enclosed Cavity Filled with Solid Obstacles, *ICHMT Digital Library Online*, 2012.
26. S. Chandrasekhar, *Radiative Transfer*, Dover Publications, New York, 1960.
27. F. Kreith, *Principles of Heat Transfer,* 7th ed., Cengage, Mason, OH, 2010.
28. K. Abe, T. Kondoh, and Y. Nagano, A New Turbulence Model for Predicting Fluid Flow and Heat Transfer in Separating and Reattaching Flows—I. Flow Field Calculations, *Int. J. Heat Mass Transfer*, vol. 37, pp. 139–151, 1994.
29. R. Abid, Evaluation of 2-Equation Turbulence Models for Predicting Transitional Flows, *Int. J. Eng. Sci.* vol. 31, pp. 831–840, Jun 1993.
30. K. C. Chang, W. D. Hsieh, and C. S. Chen, A Modified Low-Reynolds-Number Turbulence Model Applicable to Recirculating Flow in Pipe Expansion, *J. Fluids Eng. Trans. ASME*, vol. 117, pp. 417–423, Sep 1995.
31. C. K. G. Lam and K. Bremhorst, A Modified Form of the K-Epsilon Model for Predicting Wall Turbulence, *J. Fluids Eng. Trans. ASME*, vol. 103, pp. 456–460, 1981.
32. B. E. Launder and B. I. Sharma, Application of the Energy-Dissipation Model of Turbulence to the Calculation of Flow Near a Spinning Disc, *Lett. Heat Mass Transfer*, vol. 1, pp. 131–137, 1974.
33. Z. Yang and T. Shih, New Time Scale Based k-Epsilon Model for Near-Wall Turbulence, *AIAA J.*, vol. 31, pp. 1191–1198, 1993.